

# Tight-binding branch-point energies and band offsets for cubic InN, GaN, AlN and AlGaN alloys

Daniel Mourad<sup>1, a)</sup>

*Institute for Theoretical Physics, University of Bremen, Otto-Hahn-Allee 1, 28359 Bremen, Germany*

(Dated: November 9, 2018)

Starting with empirical tight-binding band structures, the branch-point (BP) energies and resulting valence band offsets (VBOs) for the zincblende phase of InN, GaN and AlN are calculated from their  $\mathbf{k}$ -averaged midgap energy. Furthermore, the directional dependence of the BPs of GaN and AlN is discussed using the Green's function method of Tersoff. We then show how to obtain the BPs for binary semiconductor alloys within a band-diagonal representation of the coherent potential approximation (CPA) and apply this method to cubic AlGaN alloys. The resulting band offsets show good agreement to available experimental and theoretical data from the literature. Our results can be used to determine the band alignment in isovalent heterostructures involving pure cubic III-nitrides or AlGaN alloys for arbitrary concentrations.

PACS numbers: 71.15.Ap, 71.20.Nr, 71.23.-k, 73.40.Kp, 78.55.Cr

## I. INTRODUCTION

Due to their wide range of potential application in optoelectronic and electronic devices, the III-nitride based semiconductor systems InN, GaN and AlN and their ternary and quaternary alloys have attracted a great deal of interest for many years now.<sup>1</sup> They can crystallize in the thermodynamically stable hexagonal configuration with a wurtzite crystal structure and in a cubic modification with a zincblende structure. Due to the low symmetry of the wurtzite system, hexagonal nitrides do not only show strain-induced, but also spontaneous polarization. The latter effect is absent in the zincblende systems: it is for example possible to eliminate the built-in fields in quantum dots by the growth of cubic III-nitride along the nonpolar (001) direction, e. g. by using GaN as dot and AlN as barrier material.<sup>2-6</sup> Furthermore, quantum well and superlattice structures based on cubic nitrides can be grown with good structural quality. AlGaN/GaN heterostructures can e. g. be used to create a two-dimensional electron gas without polarization effects.<sup>7</sup>

For the design as well as the theoretical simulation of such semiconductor devices, the knowledge of the respective valence band offsets (VBOs) across the junction of two semiconductor materials A and B is of crucial interest. In low-dimensional structures like superlattices, quantum wells or quantum dots, the confinement potential is realized by a A/B heterojunction that results in a suitable conduction band (CB) and valence band (VB) offset. Depending on the values of the respective band gaps and the resulting VBO, the electrons and holes are either located in the same ("type I" alignment) or in different spatial regions ("type II" alignment).

Furthermore, the VBO does not only determine the

geometry of the confinement potential and thus the electronic properties of low-dimensional systems. It is also relevant for the simulation of alloyed systems of the type  $A_xB_{1-x}$ , because the constituents have to be aligned along a common energy reference scale to begin with. The concentration dependence of e. g. the band gap will therefore directly depend on the energetic offset. In systems like the above mentioned AlGaN/GaN, we even find a combination of these two effects.

Although many different experimental and theoretical methods are employed to determine VBOs, the disparity in the literature values is often large. On the theoretical side, computationally costful ab initio methods<sup>8,9</sup> are ever-improving, but often still lack quantitative agreement with the experiment and do not really provide theoretical insight into the underlying formation mechanism. A different approach is presented by models that predict band discontinuities by alignment to a common energy reference like vacuum levels,<sup>10-13</sup> or different kinds of charge neutrality levels.<sup>14-19</sup> This determination of transitive "natural" VBOs represents a rather macroscopical approach that can give insight in the formation mechanism, but neglects small-scale effects like lattice mismatch or band bending on small length scales at the boundary.

In the present work, we use two approaches from the literature to determine the charge neutrality level, also known as branch point (BP), of the continuum of interface states of cubic InN, GaN and AlN with band structures from a flexible empirical tight-binding model (ETBM). We then calculate the resulting VBOs between the III-nitrides and discuss their directional dependence with the help of a Green's function method from the literature.<sup>20</sup> The experimentally observed directional independence of the cubic GaN/AlN VBO can nicely be explained in terms of our results for the BPs.

As our results for the pure systems agree well with literature data (where available), we use the coherent potential approximation (CPA) to calculate the

<sup>a)</sup> Electronic mail: [dmourad@itp.uni-bremen.de](mailto:dmourad@itp.uni-bremen.de)

concentration-dependent BP position for disordered cubic AlGa<sub>0.3</sub>N alloys and compare it to results from the simpler, but often applied virtual crystal approximation (VCA). While the VCA fails to reproduce the concentration dependence of the BP, the CPA results yield good agreement with experimental data for Al<sub>0.3</sub>Ga<sub>0.7</sub>N/GaN interfaces. Our calculated CPA BPs can be used to estimate the band alignment in interfaces with AlGa<sub>0.3</sub>N alloys for arbitrary concentrations.

## II. THEORY

### A. Branch-point energy and band alignment

The simplest linear models for the determination of VBOs across common interfaces between semiconductors use the alignment along a common reference level. An intuitive approach is the use of the vacuum level, i. e. the comparison of the electron affinities of the constituent materials.<sup>10</sup> However, the presence of interfaces and surfaces will influence the electronic properties, so that the use of values for infinite bulk crystals does not give satisfactory results for semiconductors. A large body of work deals with the refinement of this approach by establishing suitable vacuum reference levels for model solids (see the excellent review part of Ref. 21 for further reference).

Another approach that renders good results is the use of a common charge neutrality level. It is for example possible to align a broad range of materials along neutrality levels of foreign atoms like interstitial hydrogen.<sup>16</sup> In a similar manner, it is well established to employ the charge neutrality level of the continuum of interface states. These localized states develop from itinerant Bloch states, but are characterized by a complex wave vector  $\mathbf{k}$ , where  $\text{Im}(\mathbf{k})$  is normal to the plane that breaks the translational symmetry. Consequently, they decay exponentially into the other material and carry charge density across the interface, which induces an interface dipole.<sup>22</sup> The charge neutrality level of the spectrum of interface states is commonly called the branch point energy  $E_{\text{BP}}$  and is basically the crossover level between a donorlike and acceptorlike character. The Fermi level  $E_{\text{F}}$  will be pinned near the BP and the net charge density transfer due to interface states will depend on the sign and magnitude of  $E_{\text{F}} - E_{\text{BP}}$ . The (hypothetical) exact alignment of the BPs of two materials with a common interface corresponds to a band lineup where all dipole contributions cancel each other out.

In Ref. 20, Tersoff noted that  $E_{\text{BP}}$  can be calculated from the bulk properties of a semiconductor by the use of the cell-averaged real-space Green's function for the propagation along a lattice vector  $\mathbf{R}$ . This function is given as<sup>23</sup>

$$G_{\text{int}}^{\mathbf{R}}(E) = \sum_{n\mathbf{k}} \frac{e^{i\mathbf{k}\cdot\mathbf{R}}}{E - E_n(\mathbf{k})}, \quad (1)$$

with  $E_n(\mathbf{k})$  as the dispersion of the  $n$ -th band. We denote this Green's function with the subscript "int" to avoid confusion with the later introduced CPA Green's function, although the definition (1) is per se independent of any interface.

Because donor states predominantly take their spectral weight from the VB, while acceptor states likewise originate from the CB,  $E_{\text{BP}}$  can be identified as the energy where the CBs and VBs equally contribute to  $G_{\text{int}}^{\mathbf{R}}(E)$  when the interface normal is chosen parallel to the direct lattice vector  $\mathbf{R}$ . As Tersoff pointed out, it is sufficient to integrate over the three-dimensional bulk Brillouin zone (BZ) instead of separating  $\mathbf{k}_{\parallel}$  and  $\mathbf{k}_{\perp}$ , as the choice of a large enough  $\mathbf{R}$  automatically projects out the relevant contribution to  $G_{\text{int}}^{\mathbf{R}}(E)$ . This method is not applicable when the BP lies outside the band gap, however.

When the orientational dependence is small, the above mentioned approach can substantially be simplified by the use of interface-averaged approximations. In an attempt to generalize previous approaches,<sup>15,24,25</sup> Schleife et al. calculated the BP as a BZ average of the midgap energy.<sup>17</sup> Reformulated in terms of the band-resolved densities of states (DOS)<sup>26</sup>  $g_{\text{CB}}^i$  ( $g_{\text{VB}}^j$ ) for a number of  $N_{\text{CB}}$  ( $N_{\text{VB}}$ ) CBs (VBs), the BP is then approximated by

$$E_{\text{BP}} \approx \frac{1}{2} \int dE E \left[ \frac{1}{N_{\text{CB}}} \sum_i g_{\text{CB}}^i(E) + \frac{1}{N_{\text{VB}}} \sum_j g_{\text{VB}}^j(E) \right]. \quad (2)$$

This formula also holds when the BP lies in a band, as experimentally known for some small-gap materials like InAs or InN.<sup>27-29</sup> As no interface direction breaks the symmetry in Eq. (2), the BP can in principle also be obtained from the energies at the Baldereschi point,<sup>30,31</sup> see e. g. Ref. 32.

It should be noted that both methods do not only require an appropriate input band structure; in practice, the choice of a proper subset of conduction and valence bands around the band gap region is also necessary.

Strictly speaking, the knowledge of the energetic position of the BP is not sufficient to determine the VBO. In real heterojunctions between two materials A and B, the local charge neutrality condition will always be violated to some extent. The difference in the electron affinities results in a net dipole, which itself will be screened by a characteristic dielectric response  $\epsilon$ . If the BP energy  $E_{\text{BP}}$  of each material is measured with respect to its VB edge, the VBO  $\Delta E_{\text{v}}$  is obtained as

$$\Delta E_{\text{v}} = E_{\text{BP}}^{\text{B}} - E_{\text{BP}}^{\text{A}} + E_{\text{dip}}. \quad (3)$$

The magnitude of the interface dipole contribution  $E_{\text{dip}}$  can be estimated following the work of Mönch.<sup>22,32</sup> With  $X_{\text{A}}$  and  $X_{\text{B}}$  as electronegativity values from the Miedema scale, we have

$$E_{\text{dip}} = D_x(X_{\text{B}} - X_{\text{A}}), \quad (4)$$

with the phenomenological slope parameter

$$D_x = \frac{A_x}{1 + 0.1(\varepsilon_\infty - 1)^2}. \quad (5)$$

Here,  $A_x = 0.86$  eV/Miedema-unit connects the work functions and the electronegativity scale, while  $\varepsilon_\infty$  is the high-frequency dielectric constant of the semiconductor. The Miedema electronegativity values were originally defined for elementary solids.<sup>33</sup> Suitable values for binary compounds semiconductors can approximately be obtained from the geometric mean of the constituents' values, e.g. using the data from Table A.4 of Ref. 34. Note that Eq. (4) has originally been deduced for metal-semiconductor contacts<sup>35</sup> but was then found to be applicable to semiconductor interfaces, too.<sup>36</sup>

## B. Empirical tight-binding model

The importance of the choice of the band structure method in BP calculations has already been discussed in Ref. 26. It has been pointed out that a suitably parametrized empirical tight-binding model will allow for a flexible fit to a large parameter space; the input parameters can then be either chosen from experiments or from results of more sophisticated calculation schemes. They can as well deliver a more or less realistic dispersion over the whole BZ, including the Van Hove singularities at the zone boundaries, which give relevant contributions. Furthermore, due to the low computational cost, dense wave vector samples on large  $\mathbf{k}$ -space regions are effortlessly available, which is crucial to the convergence behaviour of the Green function, Eq. (1).

Throughout this paper we will use a tight-binding model based on the work of Loehr.<sup>37</sup> It makes use of a Wannier-like  $sp^3$  basis per spin direction and lattice site and can thus replicate eight doubly degenerate bands for crystals with zincblende structure. The tight-binding matrix elements of the bulk Hamiltonian  $H^{\text{bulk}}$  are

$$E_{\alpha\alpha'}^{\mathbf{R}\mathbf{R}'} = \langle \mathbf{R}\alpha | H^{\text{bulk}} | \mathbf{R}'\alpha' \rangle, \quad (6)$$

where  $\mathbf{R}$  runs over the sites of the underlying fcc Bravais lattice and  $\alpha$  is the orbital index. The band structure  $E_n(\mathbf{k})$  is obtained by the diagonalization of the matrix

$$\sum_{\alpha'} \sum_{\mathbf{R}} e^{i\mathbf{k}\cdot\mathbf{R}} E_{\alpha\alpha'}^{\mathbf{0}\mathbf{R}} \quad (7)$$

for each  $\mathbf{k} \in 1.$  BZ.

By restriction of the matrix elements to the second-nearest neighbor shell, it is possible to fit the band structure to 11 material-specific parameters, which are listed in Tab. I (the reader is referred to Refs. 26, 37, and 38 for a more detailed discussion). The fact that all bands are also fitted to the  $X$ -point energies makes it especially suitable for indirect materials, of which the properties are often not yet unambiguously established. One notable

example is AlN, which has a direct band gap in its hexagonal modification,<sup>39</sup> while an indirect  $\Gamma$ - $X$  band gap is commonly<sup>40</sup> but not always<sup>41</sup> assumed for the zincblende phase.

Note that a modification of the model such as in Ref. 26 is not necessary here, as the spin-orbit interaction is comparatively weak in the III-nitrides, which leads to spin splittings two orders of magnitude smaller than the band gap.

In order to ensure the necessary consistency among the input values (as e.g. the energetic distance of bands influences their curvature due to band-mixing effects) and simultaneously avoid the common band gap problem in ab initio calculations, we use a comprehensive set of material parameters from Fritsch et al. from empirical pseudopotential calculations (Ref. 42 for GaN and AlN, Ref. 40 for InN). The input parameters for the pseudopotentials stem from various sources which are listed in the mentioned references. In case of InN, we additionally use recent OEPx(cLDA) +  $G_0W_0$  band curvature parameters  $m_c, \gamma_1, \gamma_2, \gamma_3$  from Rinke et al.,<sup>43</sup> as their ab initio band gap for zb-InN does only deviate slightly from experimental results. Furthermore, we followed the advice of Vurgaftman and Meyer and corrected the AlN gap slightly upwards,<sup>39</sup> as the original value from Thompson et al. has originally been determined for room temperature,<sup>44</sup> while the remainder of the input parameters is assumed to be valid for low temperatures.

The resulting ETBM band structures and band-resolved densities of states for zb-GaN and zb-AlN are depicted in Fig. 1, together with the first moments /centers of gravity of the bands (the InN results are not added for the sake of clarity).

## C. Coherent potential approximation in band-diagonal representation

The CPA<sup>45-47</sup> is a well-established self-consistent Green's function method for the treatment of substitutionally disordered systems. The CPA itself and its broad scope of application is excellently described in detail in Ref. 48. For the sake of completeness, we will here only repeat the most important features.

In the standard form of the CPA, the TB Hamiltonian  $H$  of the  $A_xB_{1-x}$  alloy is separated into a site-diagonal part  $V$  and an off-diagonal part  $W$ , such that  $H = V + W$ . Here, only  $V$  is considered to be site-dependent, depending on the species on the site  $\mathbf{R}$ . The influence of the site-diagonal disorder is absorbed into the self-energy operator

$$\Sigma(z) \equiv H_{\text{eff}}(z) - W, \quad (8)$$

where  $z$  is the complex energy and  $H_{\text{eff}}(z)$  is an effective Hamiltonian; it is defined such that the configurational average  $\langle \dots \rangle$  over the resolvent of  $H$  equals the resolvent of  $H_{\text{eff}}(z)$ :

$$\langle (z\mathbf{1} - H)^{-1} \rangle \equiv [z\mathbf{1} - H_{\text{eff}}(z)]^{-1}. \quad (9)$$

Table I. Input material parameters, taken from Refs. 40, 42, and 43. See text for further details.

Parameter	Description		zb-AlN	zb-GaN	zb-InN
$a$	lattice constant	(Å)	4.38	4.52	4.98
$\Delta_{\text{SO}}$	spin-orbit splitting	(eV)	0.019	0.017	0.006
$\gamma_1$	Luttinger parameter		1.85	2.89	6.82
$\gamma_2$	Luttinger parameter		0.43	0.85	2.81
$\gamma_3$	Luttinger parameter		0.74	1.20	3.12
$m_c$	CB effective mass	( $m_0$ )	0.23	0.14	0.05
$\Gamma_1^c$ ( $\Gamma_6^c$ )	CB energy	(eV)	5.84	3.31	0.59
$\Gamma_{15}^v$	HH/LH VB energy	(eV)	0	0	0
$X_1^c$ ( $X_6^c$ )	CB energy	(eV)	5.44	4.43	4.76
$X_5^v$	HH/LH VB energy	(eV)	-2.32	-2.46	-1.48
$X_3^v$	split-off VB energy	(eV)	-5.39	-6.29	-4.80

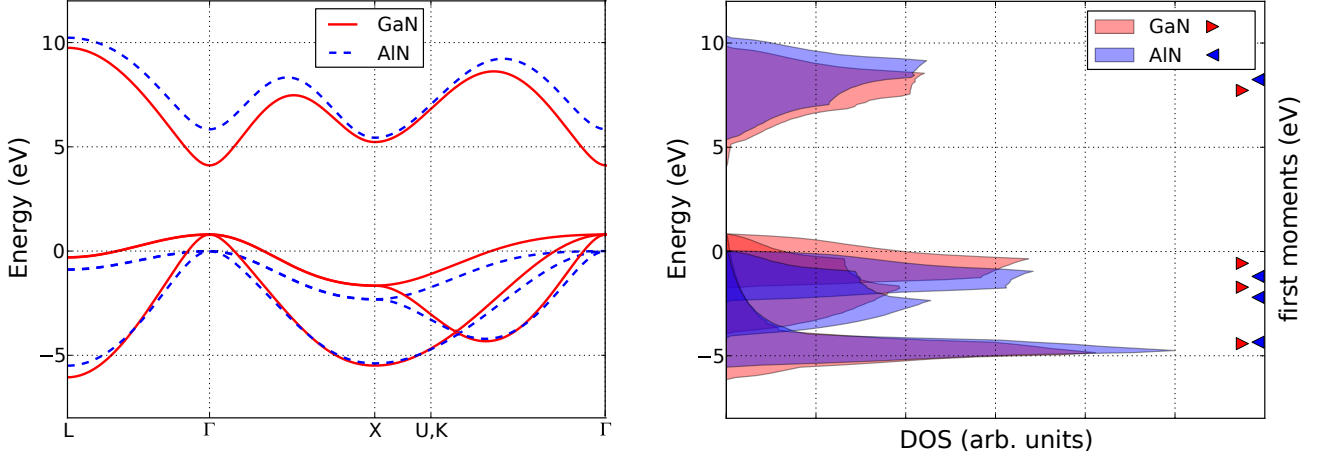


Figure 1. (Color online) ETBM band structures (left) and band-resolved DOS and first moments (right) of zb-GaN and AlN. The later calculated VBO has already been anticipated here.

When a representation is chosen, this leads to a set of self-consistency conditions for the self energies, the so-called CPA equations. In the CPA, the self-energy operator is diagonal in every representation. Additionally, its matrix elements are neither dependent on  $\mathbf{k}$  nor on  $\mathbf{R}$ .

The combination of the CPA with the here employed multiband ETBM has already been presented in Ref. 38, together with a critical discussion of the extent of its validity. This reference also describes in detail how the CPA self-energy and Green's function can properly be transformed from the localized  $sp^3$  basis to a band-diagonal representation. The latter, in which  $H_{\text{eff}}$  is diagonal in  $\mathbf{k}$ , is crucial for the calculation of BPs for the alloyed system, as one has to restrict the calculation to a subset of bands and the most natural choice of band index  $n$  is their energetic hierarchy.

In the here employed form, the CPA only maps the substitutional disorder in the first moments / centers of gravity  $E_{A/B}^0$  of the constituents on the self energy  $\Sigma^n(z)$ ,

$$E_{n,A/B}^0 = \int dE E g_{A/B}^n(E) \xrightarrow{\text{CPA}} \Sigma^n(z), \quad (10)$$

where  $g_{A/B}^n$  is again the band-resolved DOS (normed to unity). The off-diagonal disorder effects are simulated in the VCA, i.e. interpolated linearly with the concentration  $x$ . The self-consistent iteration scheme for the CPA equations as described in detail in Sec. II of Ref. 38 finally leaves us with the CPA Green's function. Using its  $\mathbf{k}$ -representation  $G_{\text{CPA}}^{n\mathbf{k}}$ , we can then extract the CPA one-particle spectral function  $S_{\text{CPA}}^{n\mathbf{k}}$  and DOS  $g_{\text{CPA}}^n(E)$ :

$$S_{\text{CPA}}^{n\mathbf{k}}(E) = -\frac{1}{\pi} \lim_{\delta \searrow 0} \text{Im} G_{\text{CPA}}^{n\mathbf{k}}(E + i\delta), \quad (11)$$

$$g_{\text{CPA}}^n(E) = -\frac{1}{\pi N_{\mathbf{k}}} \lim_{\delta \searrow 0} \text{Im} \sum_{\mathbf{k}} G_{\text{CPA}}^{n\mathbf{k}}(E + i\delta). \quad (12)$$

Here,  $\delta \in \mathbb{R}$  and  $N_{\mathbf{k}}$  is the number of wave vector values in the irreducible wedge.

Although the CPA can simulate many effects that go beyond the scope of static mean-field treatments like the VCA (such as spectral broadening due to finite lifetimes or band gap bowing), it also has several limitations. Due to the translational invariance of  $H_{\text{eff}}$ , the CPA cannot simulate local strain patterns. It will therefore only yield reliable results if the difference of the lattice constants is rather small. Besides this constraint, the CPA can be shown<sup>48</sup> to yield very good results in two limit cases:

(1) The *weak scattering limit*, where the difference of the first moments of the A and B bands is smaller than the respective bandwidths.

(2) The *split band limit*, where these first moments are either far apart and/or the bandwidths are small enough for the bands of A and B to not overlap.

#### D. Calculation of branch points in the coherent potential approximation

The approximated branch point energies for alloys can also be calculated from the ETBM+CPA results. We first define the complex quasi-particle band structure

$$E_n^{\text{CPA}}(\mathbf{k}) \equiv \langle \mathbf{k}n | H_{\text{eff}} | \mathbf{k}n \rangle \\ = \langle \mathbf{k}n | W | \mathbf{k}n \rangle + \Sigma^n(z = E_n^{\text{CPA}}), \quad (13)$$

where  $|\mathbf{k}n\rangle$  are Bloch states which diagonalize  $H_{\text{eff}}$ . Now the interface Green's function for the alloy can obviously be defined by using  $E_n^{\text{CPA}}(\mathbf{k})$  as dispersion in Eq. (1). As the CPA Green's function itself is given by

$$G_{\text{CPA}}^{m\mathbf{k}}(z) = \langle \mathbf{k}n | [z\mathbb{1} - H_{\text{eff}}(z)]^{-1} | \mathbf{k}n \rangle, \quad (14)$$

the interface Green's function can directly be obtained by means of a discrete Fourier transformation:

$$G_{\text{int}}^{\mathbf{R}}(E) = \sum_{n\mathbf{k}} e^{i\mathbf{k}\cdot\mathbf{R}} [E - E_n^{\text{CPA}}(\mathbf{k})]^{-1} \\ = \sum_{n\mathbf{k}} e^{i\mathbf{k}\cdot\mathbf{R}} G_{\text{CPA}}^{m\mathbf{k}}(E). \quad (15)$$

Like in the pure case, the BP has to lie in a real gap of the quasi-particle band structure. As  $G_{\text{CPA}}^{m\mathbf{k}}$  has no poles in this region, the calculation can be restricted to the real part of the energy axis.

When the BZ average approach from Eq. (2) is used, the band-resolved densities of states can analogously be replaced by their CPA counterparts from Eq. (12).

### III. RESULTS

#### A. Pure zincblende III-nitrides

In order to calculate the BP energies from the TB band structures, we follow the recommendations of Schleife et al.<sup>17</sup> and use one CB and the two uppermost VBs per spin direction. As Fig. 1 suggests, this band subset can

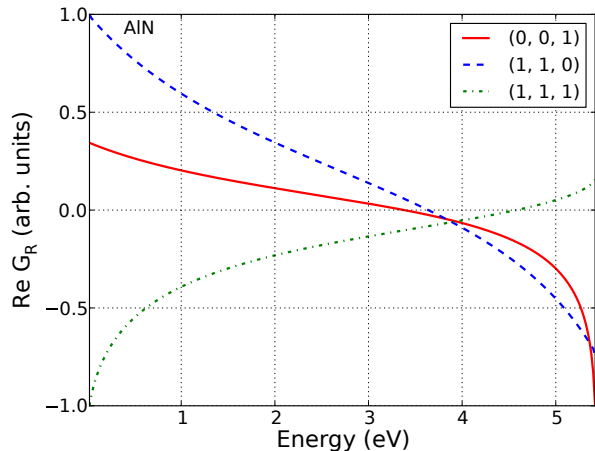


Figure 2. (Color online) Real part of  $G_{\text{int}}^{\mathbf{R}}$  for AlN for the (001), (110) and (111) direction.

be justified by the much larger dispersion of the lowest VB. It should however be kept in mind that this set is obviously not suitable for several II-VI materials,<sup>26</sup> and the choice of bands certainly remains a major source of uncertainties in the BP calculation. For that reason, we carefully recommend the same uncertainty range of 0.2 eV as given by Schleife et al.

For the BZ average method, convergency of the results for  $E_{\text{BP}}$  is easily achieved by using a moderately dense  $\mathbf{k}$ -grid on the irreducible wedge, so that a reduction to the Baldereschi point does not render any practical advantage. Convergency within 10 meV could be obtained with an equidistant resolution of about 100–200  $\mathbf{k}$ -values between  $\Gamma$  and  $X$ .

The interface Green's function however is known to be extremely difficult to converge.<sup>17,26</sup> In practice, it turned out that very dense wave vector samples on the full BZ are necessary. Figure 2 exemplarily shows the real part of  $G_{\text{int}}^{\mathbf{R}}$  for AlN for three different interface orientations  $\mathbf{R} \propto (001)$ ,  $(110)$  and  $(111)$ . As explained in Sec. II A, the BP can be obtained by the zero-crossing of this curve, which should arise for large enough multiples of  $\mathbf{R}$ . For GaN and AlN, the intersections could be brought to convergency within 20 meV for the (001) and (110) direction when  $\sim 250$ – $300$   $\mathbf{k}$ -values were used between  $\Gamma$  and  $X$ . However, satisfactory convergency for the (111) direction could not be achieved for either material.

In case of InN, the results from the BZ average method render a BP energy in the CB region, so that the Green's function method is not applicable. This is also in agreement with theoretical and experimental results from the literature.<sup>28</sup>

The results for the BP energies  $E_{\text{BP}}$  for the cubic III-nitrides InN, GaN and AlN can be found in Tab. II, together with several theoretical and experimental results from the literature. Further information on the respective source is provided in the footnotes of the table.



Table II. Branch point energies  $E_{BP}$  for cubic III-nitrides in eV.

Material	$E_g$	$E_{BP}$			
		$\mathbf{R} \propto (001)$	$\mathbf{R} \propto (110)$	BZ average	Literature
zb-AlN	5.44	3.38	3.64	3.28	2.97 <sup>a</sup> ; 3.19±0.18 <sup>b</sup>
zb-GaN	3.31	2.62	2.86	2.50	2.37 <sup>a</sup> ; 2.34±0.09 <sup>b</sup> ; 2.31 <sup>c</sup>
zb-InN	0.59	—	—	1.65	1.51 <sup>a</sup> ; 1.59±0.26 <sup>b</sup> ; 1.50 <sup>d</sup> ; 1.38±0.1 <sup>e</sup>

<sup>a</sup> ETBM + BZ average calculation, Ref. 32, no explicit specification on bulk parameters.

<sup>b</sup> Empirical value from fit to experimental band offsets, Ref. 19.

<sup>c</sup> Quasiparticle BZ average calculation with  $E_g = 3.28$  eV (HSE03+ $G_0W_0$ ), Ref. 17.

<sup>d</sup> Quasiparticle BZ average calculation with  $E_g = 0.47$  eV (HSE03+ $G_0W_0$ ), Ref. 17.

<sup>e</sup> XPS measurement on (001) surface at room temperature, Ref. 49.

However, it should be noted that the energy gap of the theoretical literature values does in general not coincide with our input parameter set. Furthermore, no direction-dependent BP energies are available to our knowledge. Still, our calculated values agree reasonably well with the external data. For the sake of completeness, it should be noted that Ref. 50 contains further theoretical values for the cubic III-nitrides that were obtained from slightly different ab initio band energies, but also show good agreement.

Our results also show that the position of  $E_{BP}$  carries a clear-cut directional dependency, where

$$E_{BP}(\text{BZ average}) < E_{BP}(001) < E_{BP}(110)$$

for both GaN and AlN. Additionally, the trend of the available data for the (111) direction (see again Fig. 2) also suggests that

$$E_{BP}(111) > E_{BP}(110) > E_{BP}(001)$$

might hold. Whether the "real" directional average of the BP in these materials lies energetically below the (001) and (110) values or the BZ average method just gives a slightly too low  $E_{BP}$ , cannot ultimately be concluded from our calculations, as reliable results for further directions would be necessary.

With knowledge of the BP energies, the band alignment can now be calculated from Eqs. (3)-(5). For the contribution of the interface dipole, the electronegativity values from Ref. 34 have been used. As the localized interface states exponentially decay into the energy barrier caused by the VBO, we used the dielectric constant  $\epsilon_\infty(\text{InN}) = 7.0$ <sup>52</sup> for both the InN/AlN and InN/GaN junction and  $\epsilon_\infty(\text{GaN}) = 5.3$ <sup>53</sup> for GaN/AlN. The results for the BP difference, the dipole contribution and the resulting VBO can be found in Tab. III, together with theoretical and experimental values from the literature.

For all interfaces, the contribution of the dipole correction is small, so that an approximate alignment of these three systems along the BP energy is well justified. This is in agreement with general considerations in the literature on junctions between cubic binary semiconductor compounds.<sup>20,22</sup>

For the GaN/AlN interface, the VBO is practically independent of the interface orientation. This fact might

seem strange at first glance, as the zincblende (001) interface is polar, while the (110) is not. However, this result is in compliance with various experimental and theoretical findings (see e. g. Ref. 39) and has also been deduced by Lambrecht and Segall<sup>21</sup> from an analysis of the bonding geometry and polarity at isovalent zincblende interfaces. Our calculations show that this independence can also be deduced from band-structure related properties, as the difference in the (001) and (110) BP energies is almost identical (see again Tab. II).

Notably, the BZ average method also gives the same BP difference and thus VBO, which underlines its suitability for material systems with weak directional dependence. Although no directionally dependent calculation could be performed for InN, the detailed analysis of Lambrecht and Segall indicates that the same behavior will also hold for InN.

From a quantitative point of view, the VBOs agree quite well with available data from the literature. Our value of  $\Delta E_{VB}(\text{GaN/AlN}) \approx 0.8$  eV agrees with the recommendation from the topical review of Vurgaftman and Meyer<sup>39</sup> and also with the comprehensive experimental analysis of Mönch.<sup>19</sup> The theoretical value of 0.6 eV from Mönch also stems from ETBM calculations, but with the use of atomic term values and hopping matrix elements from 1972 and 1981, respectively.<sup>54,55</sup> The smallest literature value of  $0.5 \pm 0.1$  eV has been determined from lattice-matched quantum wells on 3C-SiC substrate at room temperature. For both InN/AlN and InN/GaN, our results also agree well with the literature, only the review by Vurgaftman et al. recommends smaller values. This could be explained by the fact that their publication is from 2003, when high-quality wurtzite as well as zincblende InN samples did not yet exist for a long time.

The overall resulting band lineup as recommended by us for the cubic phases of InN, GaN and AlN is depicted in Fig. 3.

## B. AlGaN alloys with zincblende phase

In contrast to InGaN and InAlN, the lattice mismatch between the constituents in cubic AlGaN is relatively small with 3%, which suggests that the influence of local

Table III. Resulting valence band offsets  $\Delta E_{\text{VB}}(A/B)$  for cubic nitrides in eV.

Interface A/B	$E_{\text{BP}}^{\text{B}} - E_{\text{BP}}^{\text{A}}$			Dipole	$\Delta E_{\text{VB}}(A/B)$	
	$\mathbf{R} \propto (001)$	$\mathbf{R} \propto (110)$	BZ average		This work	Literature
GaN/AlN	0.76	0.78	0.78	+ 0.02	0.78, 0.80	$0.5 \pm 0.1^{\text{a}}$ , $0.6^{\text{b}}$ , $0.8^{\text{c}}$ , $0.85^{\text{d}}$
InN/AlN	—	—	1.63	+ 0.03	1.66	$1.1^{\text{c}}$ , $1.46^{\text{b}}$ , $1.60^{\text{d}}$
InN/GaN	—	—	0.85	+ 0.02	0.87	$0.3^{\text{c}}$ , $0.75^{\text{d}}$ , $0.81^{\text{e}}$ , $0.86^{\text{b}}$

<sup>a</sup> Combination of intersubband and interband spectroscopies and ab initio HSE06 +  $G_0W_0$  calculations on GaN/AlN quantum wells with lattice-matched AlN from Ref. 51.

<sup>b</sup> ETBM + BZ average calculation, Ref. 32, no explicit specification on bulk parameters.

<sup>c</sup> Estimated after analysis of various experimental and theoretical sources, Ref. 39.

<sup>d</sup> Difference of branch points from Ref. 19, see footnote of Tab. II. This should only be considered a rough estimate, as the branch points were originally obtained the opposite way around.

<sup>e</sup> Difference of branch points from Ref. 17, see footnotes of Tab. II.

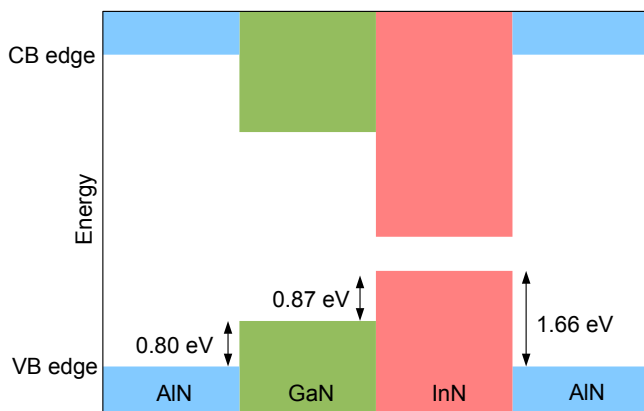


Figure 3. (Color online) Band lineup for the zincblende modification of the III-nitrides. The small deviation from the intransitivity between the GaN/AlN, InN/GaN and the InN/AlN VBO originates from interface dipole effects (see text).

lattice distortions is not of major importance when the electronic structure of the alloy is calculated.

In fact, it has already been shown in Ref. 38 that the CPA gives good agreement with supercell calculations and further literature values for the  $\Gamma$ -valley bowing and the crossover concentration between a direct GaN-dominated and indirect AlN-dominated behavior. Besides a small variation in the band curvatures, which is not relevant for the here discussed properties, those calculations were performed for an almost identical parameter set and the same VBO (albeit by chance, as the value of  $\Delta E_{\text{VB}}(\text{GaN/AlN}) \approx 0.8 \text{ eV}$  calculated in this paper coincides with the there employed recommendation from Vurgaftman and Meyer). A closer look at the bandwidths and the position of the first band moments as depicted on the right of Fig. 1 shows that this system is very close to the weak scattering limit, which also underlines the applicability of the CPA. Furthermore, recent experimental data for the band alignment is available,

in particular for cubic nonpolar  $\text{Al}_{0.3}\text{Ga}_{0.7}\text{N}/\text{GaN}$  heterostructures, which were grown by means of molecular beam epitaxy on 3C-SiC (001). In Ref. 7, Wei et al. report on a two-dimensional electron gas at this interface and observe a large conduction-to-valence band offset ratio of 5:1 which enhances the electron accumulation.

As the electronic structures of two materials A and B enter the calculation for alloys, an energy offset and thus VBO between A and B has also to be established as input parameter. In general, the choice of a VBO for CPA or supercell calculations for alloys is far from trivial. With varying concentration  $x$  in the  $\text{A}_x\text{B}_{1-x}$  alloy, the outline of the problem does in principle change from single-impurity-like behavior over dilute systems up to whole A-in-B-clusters, so that the "true" VBO should in principle be concentration- as well as lattice-site-dependent. Nevertheless, the usage of a fixed parameter is common for the sake of simplicity. In case of the AlGaN system under consideration, we will use the interface VBO of 0.8 eV, as it has been shown to be directionally independent in the last section and gives the correct limit in the pure and in the phase separation case.

The resulting CPA quasiparticle band structure for  $\text{Al}_{0.3}\text{Ga}_{0.7}\text{N}$  is depicted in Fig. 4. Note that the linewidths were artificially enlarged for enhanced contrast in this figure. For vanishing imaginary part in the complex energy  $z = E + i\delta$ , an unambiguous CB edge and VB edge and thus band gap can be identified.

In order to obtain the position of the BP over the whole concentration range, a small imaginary part of  $\delta = 10^{-4} \text{ eV}$  and  $\#\mathbf{k} \approx 10^7$  values in the irreducible wedge have been used in the CPA iterations, together with an energy resolution of  $\Delta z = 5 \times 10^{-3} \text{ eV}$ . In the following, we restrict the discussion to the results of the BZ average approach as defined in Eq. (12) for two reasons:

(1) The almost identical energy difference for pure GaN and AlN between  $E_{\text{BP}}(\text{BZ average})$ ,  $E_{\text{BP}}(001)$  and  $E_{\text{BP}}(110)$  of 0.1 and 0.25 eV, respectively, directly carries over to the results for AlGaN when the quasiparticle band structure is used according to Eq. (15). This holds in good approximation over the whole concentra-

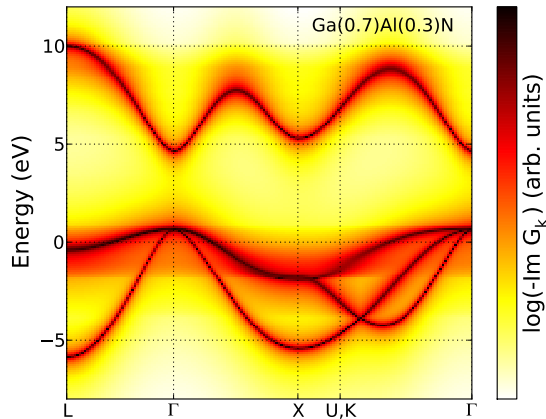


Figure 4. (Color online) CPA quasiparticle band structure for  $\text{Al}_{0.3}\text{Ga}_{0.7}\text{N}$ .

tion range. Due to the very slow convergency, this has only been spot-checked with a lower energy resolution.

(2) In real materials, disorder effects will prevent any translational invariance, which is an artificial symmetry of the CPA Hamiltonian. It is therefore at least questionable whether effects that strongly originate from symmetry properties of the quasiparticle band structure carry over to the behavior at real disordered interfaces.

In addition, virtual crystal calculations have also been performed for comparison, as the VCA is also used in the literature to calculate branch-point energies of alloys,<sup>32</sup> supposedly due to its simplicity. Here, the matrix elements of the alloy with concentration  $x$  are obtained by a linear interpolation between the pure values. As the VCA is contained in the CPA as a limit case,<sup>48</sup> the CPA results serve as a benchmark for the reliability of the VCA.

The resulting band edges and BPs of AlGaN can be found in Fig. 5. Here, the same band subset as in the pure case was used for all concentrations, but for material combinations close to the split-band limit, an individual and concentration-dependent choice might be necessary. It is immediately evident that the position of the CPA as well as the VCA BP is almost constant on the common energy scale of the  $\text{A}_x\text{B}_{1-x}$  alloy, so that the relevant value for band alignment, the energetic distance between the BP and the VB edge, is only determined by the latter. This behavior originates in the use of a constant A-to-B VBO that has itself been determined by the alignment of BPs and will not hold when either a concentration-dependent VBO and/or a VBO with large dipole contribution is used in the calculations.

A comparison of the CPA to the VCA results reveals that the latter gives slightly too low VB edges. In Fig. 6, the relative BP position  $E_{\text{BP}}(x) - E_{\text{VB}}(x)$  is depicted as a function of the concentration  $x$ . While the VCA erroneously yields an almost linear behavior, the relative

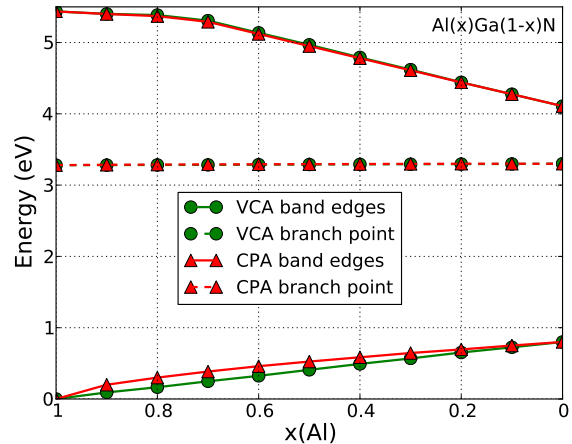


Figure 5. (Color online). CB edge, VB edge and BP energy of AlGaN, calculated in the CPA and the VCA from the TB band structures, respectively. The VCA results for the BP and the CB edge are overlaid by the CPA data.

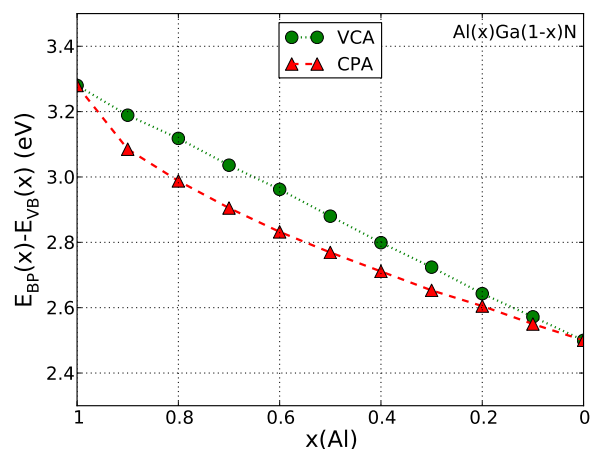


Figure 6. (Color online) Relative BP position  $E_{\text{BP}}(x) - E_{\text{VB}}(x)$  of AlGaN calculated in the CPA and the VCA.

CPA BP position shows a pronounced bowing, where a satisfactory fit by a quadratic or cubic function is not possible for the whole concentration range. Table IV comprehensively lists the band edges and the relative BP energy of zb-AlGaN. These values can be used to estimate the band alignment for all concentrations with respect to any material whose branch points are known. Like in the pure case, the uncertainty will at least be 0.2 eV, not including additional deviations due to the use of the CPA.

We will finally compare our results to the work of Wei et al. for cubic  $\text{Al}_{0.3}\text{Ga}_{0.7}\text{N}/\text{GaN}$  heterostructures.<sup>7</sup> The difference in the electrostatic potential at the interface, which is determined by means of electron holography, gives a CB offset of 0.65 eV in their experiment. To-



Table IV. Concentration-dependent VB and CB edge  $E_{\text{VB/CB}}$ , and relative BP position  $E_{\text{BP}} - E_{\text{VB}}$  for zb-AlGaN as obtained in the CPA. All values in eV.

	$x$ (Al)	$E_{\text{VB}}$	$E_{\text{CB}}$	$E_{\text{BP}} - E_{\text{VB}}$
AlN	1	0	5.44 <sup>†</sup>	3.28
	0.9	0.20	5.40	3.09
	0.8	0.30	5.37	2.99
	0.7	0.39	5.29	2.91
	0.6	0.46	5.12	2.83
	0.5	0.53	4.95	2.77
	0.4	0.59	4.78	2.71
	0.3	0.65	4.61	2.65
	0.2	0.70	4.44	2.61
GaN	0	0.80	4.11 <sup>†</sup>	2.50

<sup>†</sup> Input values from parametrization, see Tab. I.

gether with a measured band gap difference of 0.78 eV across the junction, this yields a VB offset of 0.13 eV. The value is in very good agreement with our theoretical result of  $2.65 \text{ eV} - 2.50 \text{ eV} = 0.15 \text{ eV}$ . However, this compliance definitely exceeds the predictive power of the calculations. When combined, our BP and band gap results for this material combination give a conduction-to-valence-band ratio of  $0.5/0.15 \approx 3.3$ , which is below the experimental value of 5. The deviation can be traced back to their spectroscopically determined band gap difference between  $\text{Al}_{0.3}\text{Ga}_{0.7}\text{N}$  and GaN, which is larger than our calculated band gap difference of 0.65 eV. Also, our calculations do not include any effects from lattice strain, which, albeit small, will also influence the results. Notably, the AlGaN layer thickness in their experiment is only 30 nm, so that finite size effects will also likely play a role. Furthermore, the authors notice composition fluctuations and oxygen contamination in their samples. If we account for these effects by using the same modified band gap difference of 0.78 eV in our calculations, we arrive at a ratio of 4.2, which is surprisingly good, especially when the various sources of uncertainty are considered on both the theoretical and the experimental side.

#### IV. SUMMARY

In this paper, we showed that the branch-point (BP) energies and resulting band alignment for the cubic III-nitrides InN, GaN and AlN can be calculated from tight-binding band structures with consistent and up-to-date input parameters. The directional independence of the valence band offset (VBO) at the unstrained GaN/AlN interface has been traced back to a constant shift of the corresponding BPs by the use of Tersoff's Green's function method. We then showed how the coherent potential approximation (CPA) can be used in combination with the tight-binding model to obtain the BPs

and VBOs for alloyed systems and applied this method to the zincblende modification of AlGaN over the whole concentration range. While a virtual crystal treatment of the system gives erroneous results, the CPA agrees well with experimental data on  $\text{Al}_{0.3}\text{Ga}_{0.7}\text{N}/\text{GaN}$  heterostructures. Our results can be used to determine the band alignment in isovalent heterostructures involving pure cubic III-nitrides or AlGaN alloys for arbitrary concentrations.

#### ACKNOWLEDGMENTS

The author would like to thank G. Czycholl for interesting discussions and the introduction to the CPA. The author also thankfully acknowledges the developers of the free Python numpy and matplotlib modules, which were used for calculation and visualization.

#### REFERENCES

- F. A. Ponce and D. P. Bour, *Nature (London)* **386**, 351 (1997).
- E. Martinez-Guerrero, C. Adelman, F. Chabuel, J. Simon, N. T. Pelekanos, G. Mula, B. Daudin, G. Feuillet, and H. Mariette, *Appl. Phys. Lett.* **77**, 809 (2000).
- B. Daudin, G. Feuillet, H. Mariette, G. Mula, N. Pelekanos, E. Molva, J.-L. Rouvière, C. Adelman, E. Martinez, Guerrero, J. Barjon, F. Chabuel, B. Bataillou, and J. Simon, *Jpn. J. Appl. Phys.* **40**, 1892 (2001).
- N. Gogneau, F. Enjalbert, F. Fossard, Y. Hori, C. Adelman, J. Brault, E. Martinez-Guerrero, J. Simon, E. Bellet-Amalric, D. Jalabert, N. Pelekanos, J.-L. Rouvière, B. Daudin, L. S. Dang, H. Mariette, and E. Monroy, *phys. stat. sol. (c)* **1**, 1445 (2004).
- D. Lagarde, A. Balocchi, H. Carrère, P. Renucci, T. Amand, S. Founta, H. Mariette, and X. Marie, *Microelectron. J.* **40**, 328 (2009).
- J. Simon, N. T. Pelekanos, C. Adelman, E. Martinez-Guerrero, R. André, B. Daudin, L. S. Dang, and H. Mariette, *Phys. Rev. B* **68**, 035312 (2003).
- Q. Y. Wei, T. Li, J. Y. Huang, F. A. Ponce, E. Tschumak, A. Zado, and D. J. As, *Appl. Phys. Lett.* **100**, 142108 (2012).
- S.-H. Wei and A. Zunger, *Appl. Phys. Lett.* **72**, 2011 (1998).
- P. G. Moses, M. Miao, Q. Yan, and C. G. Van de Walle, *J. Chem. Phys.* **134**, 084703 (2011).
- R. Anderson, *Solid-State Electron.* **5**, 341 (1962).
- J. A. Van Vechten, *Phys. Rev.* **187**, 1007 (1969).
- C. G. Van de Walle and R. M. Martin, *Phys. Rev. B* **34**, 5621 (1986).
- C. G. Van de Walle, *Phys. Rev. B* **39**, 1871 (1989).
- W. A. Harrison and J. Tersoff, *J. Vac. Sci. Technol. B* **4**, 1068 (1986).
- M. Cardona and N. E. Christensen, *Phys. Rev. B* **35**, 6182 (1987).
- C. G. Van de Walle and J. Neugebauer, *Nature* **423**, 626 (2003).
- A. Schleife, F. Fuchs, C. Rödl, J. Furthmüller, and F. Bechstedt, *Appl. Phys. Lett.* **94**, 012104 (2009).
- B. Höfling, A. Schleife, F. Fuchs, C. Rödl, and F. Bechstedt, *Appl. Phys. Lett.* **97**, 032116 (2010).
- W. Mönch, *J. Appl. Phys.* **109**, 113724 (2011).
- J. Tersoff, *Phys. Rev. B* **30**, 4874 (1984).
- W. R. L. Lambrecht and B. Segall, *Phys. Rev. B* **41**, 2832 (1990).
- W. Mönch, *Electronic Properties of Semiconductor Interfaces*, 1st ed. (Springer, Berlin/Heidelberg, 2004).
- R. E. Allen, *Phys. Rev. B* **20**, 1454 (1979).
- F. Flores and C. Tejedor, *J. Phys. C* **12**, 731 (1979).
- J. Tersoff, *Phys. Rev. B* **32**, 6968 (1985).

- <sup>26</sup>D. Mourad, J.-P. Richters, L. Gérard, R. André, J. Bleuse, and H. Mariette, *Phys. Rev. B* **86**, 195308 (2012).
- <sup>27</sup>M. Noguchi, K. Hirakawa, and T. Ikoma, *Phys. Rev. Lett.* **66**, 2243 (1991).
- <sup>28</sup>I. Mahboob, T. D. Veal, L. F. J. Piper, C. F. McConville, H. Lu, W. J. Schaff, J. Furthmüller, and F. Bechstedt, *Phys. Rev. B* **69**, 201307 (2004).
- <sup>29</sup>L. F. J. Piper, T. D. Veal, M. J. Lowe, and C. F. McConville, *Phys. Rev. B* **73**, 195321 (2006).
- <sup>30</sup>A. Baldereschi, *Phys. Rev. B* **7**, 5212 (1973).
- <sup>31</sup>D. J. Chadi and M. L. Cohen, *Phys. Rev. B* **8**, 5747 (1973).
- <sup>32</sup>W. Mönch, *J. Appl. Phys.* **80**, 5076 (1996).
- <sup>33</sup>A. Miedema, P. de Châtel, and F. de Boer, *Physica B+C* **100**, 1 (1980).
- <sup>34</sup>W. Mönch, *Semiconductor Surfaces and Interfaces* (Springer-Verlag, Berlin/Heidelberg, 2001).
- <sup>35</sup>W. Mönch, *Appl. Surf. Sci.* **92**, 367 (1996).
- <sup>36</sup>W. Mönch, *Appl. Phys. Lett.* **91**, 042117 (2007).
- <sup>37</sup>J. P. Loehr, *Phys. Rev. B* **50**, 5429 (1994).
- <sup>38</sup>D. Mourad and G. Czycholl, *Eur. Phys. J. B* **85**, 153 (2012).
- <sup>39</sup>I. Vurgaftman and J. R. Meyer, *J. Appl. Phys.* **94**, 3675 (2003).
- <sup>40</sup>D. Fritsch, H. Schmidt, and M. Grundmann, *Phys. Rev. B* **69**, 165204 (2004).
- <sup>41</sup>V. A. Fonoberov and A. A. Balandin, *J. Appl. Phys.* **94**, 7178 (2003).
- <sup>42</sup>D. Fritsch, H. Schmidt, and M. Grundmann, *Phys. Rev. B* **67**, 235205 (2003).
- <sup>43</sup>P. Rinke, M. Winkelkemper, A. Qteish, D. Bimberg, J. Neugebauer, and M. Scheffler, *Phys. Rev. B* **77**, 075202 (2008).
- <sup>44</sup>M. P. Thompson, G. W. Auner, T. S. Zheleva, K. A. Jones, S. J. Simko, and J. N. Hilfiker, *J. Appl. Phys.* **89**, 3331 (2001).
- <sup>45</sup>P. Soven, *Phys. Rev.* **156**, 809 (1967).
- <sup>46</sup>D. W. Taylor, *Phys. Rev.* **156**, 1017 (1967).
- <sup>47</sup>Y. Onodera and Y. Toyozawa, *J. Phys. Soc. Jpn.* **24**, 341 (1968).
- <sup>48</sup>T. Matsubara, H. Matsuda, T. Murao, T. Tsuneto, and F. Yonezawa, *The Structure and Properties of Matter*, edited by T. Matsubara (Springer-Verlag, Berlin/Heidelberg, 1982).
- <sup>49</sup>P. D. C. King, T. D. Veal, C. F. McConville, F. Fuchs, J. Furthmüller, F. Bechstedt, P. Schley, R. Goldhahn, J. Schörmann, D. J. As, K. Lischka, D. Muto, H. Naoi, Y. Nanishi, H. Lu, and W. J. Schaff, *Appl. Phys. Lett.* **91**, 092101 (2007).
- <sup>50</sup>A. Belabbes, L. C. de Carvalho, A. Schleife, and F. Bechstedt, *Phys. Rev. B* **84**, 125108 (2011).
- <sup>51</sup>C. Mietze, M. Landmann, E. Rauls, H. Machhadani, S. Sakr, M. Tchernycheva, F. H. Julien, W. G. Schmidt, K. Lischka, and D. J. As, *Phys. Rev. B* **83**, 195301 (2011).
- <sup>52</sup>P. Schley, R. Goldhahn, C. Napierala, G. Gobsch, J. Schörmann, D. J. As, K. Lischka, M. Feneberg, and K. Thonke, *Semicond. Sci. Technol.* **23**, 055001 (2008).
- <sup>53</sup>M. E. Levinshtein, S. L. Rumyantsev, and M. S. Shur, *Properties of Advanced Semiconductor Materials: GaN, AlN, InN, BN, SiC, SiGe: GaN, AlN, InN, BN, SiC, SiGe*, 1st ed. (John Wiley & Sons, NY-Chichester-Weinheim-Brisbane-Singapore-Toronto, 2001).
- <sup>54</sup>C. F. Fischer, *At. Data. Nucl. Data Tables* **4**, 301 (1972).
- <sup>55</sup>W. A. Harrison, *Phys. Rev. B* **24**, 5835 (1981).